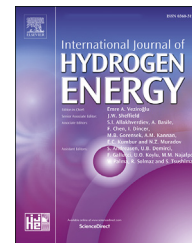




ELSEVIER

Available online at www.sciencedirect.com

ScienceDirect

journal homepage: www.elsevier.com/locate/he

Synthesizing of SnS₂ photocatalyst from SnO₂ powders by thermal sulfurization with varying temperature (400 °C and 500 °C) and time

Alaaddin Cem Ok, Cevat Sarioğlu*

Marmara University, Faculty of Engineering, Metallurgical and Materials Engineering Department, TR34722, Istanbul, Turkey

HIGHLIGHTS

- SnS₂ successfully synthesized from SnO₂ powders by thermal sulfurization method.
- Hexagonal SnS₂ powders obtained after optimization of sulfurization temperature and time.
- SnS₂ photocatalysis exhibited 2.5 μA/cm² photo current greater than literature values.

ARTICLE INFO

Article history:

Received 25 January 2023
Received in revised form
31 July 2023
Accepted 11 August 2023
Available online xxx

Keywords:

Tin disulfide
Photocatalyst
Solar energy
Water splitting
Hydrogen production
Thermal sulfurization

ABSTRACT

SnS₂ from SnO₂ powders was successfully produced by the thermal sulfurization method to obtain pure SnS₂ powders by varying the sulfurization temperature and time. XRD analysis confirmed pure hexagonal SnS₂ powders at 400 and 500 °C after 24 h of sulfurization. Grain size analysis in SEM indicated that the average grain size of powders synthesized at 400 °C and 500 °C were 1 and 11 μm, respectively. The band gap values of the obtained powders at 400 and 500 °C was determined by UV–vis spectroscopy as 2.26 eV and 2.24 eV, respectively. The photoelectrochemical analysis of the SnS₂ photoelectrode produced at 500 °C revealed a flat band potential of −0.50 V, a charge carrier density of $1.49 \times 10^{20} \text{ cm}^{-3}$ and photocurrent density of 2.5 μA/cm² at 0 V vs SCE. These results indicated that SnS₂ synthesized for the first time by the thermal sulfurization technique from SnO₂, which was a simple and cheap technique, was a promising candidate to be used as a photocatalysts.

© 2023 Hydrogen Energy Publications LLC. Published by Elsevier Ltd. All rights reserved.

1. Introduction

Hydrogen can be a solution to the climate crisis, as stated by the latest decision taken by the European Parliament and the Council on June 30, 2021. Hydrogen is one of the leading sources of renewable energy as an alternative to fossil fuels.

Hydrogen is produced from both renewable and nonrenewable sources of energy. However, using non-renewable energy sources in hydrogen production will cause greenhouse gas emissions and global warming. The production of H₂ by splitting water with solar energy as a renewable energy source through photocatalytic and photo-electrochemical methods

* Corresponding author.

E-mail addresses: cem.ok@marmara.edu.tr (A.C. Ok), cevat.sarioğlu@marmara.edu.tr (C. Sarioğlu).

<https://doi.org/10.1016/j.ijhydene.2023.08.147>

0360-3199/© 2023 Hydrogen Energy Publications LLC. Published by Elsevier Ltd. All rights reserved.

has great potential to be an alternative energy source to satisfy the world's energy needs [1–5].

Photocatalysts are semiconductor materials that are activated by light energy and initiate a series of electrochemical reactions. Many photocatalytic semiconductor materials have been studied, such as metal oxides, metal nitrides, oxynitrides, metal sulfides, and organic materials. Metal oxides (e.g., TiO_2) have suitable band structures that provide the thermodynamic requirements for splitting water, and they are resistant to photo-corrosion.

However, they are active under ultraviolet light, which constitutes 4% of the solar spectrum due to its wide band gap value, and because of this they have very low efficiency, which limits their uses [6,7]. On the other hand, metal sulfide (CdS , ZnS , CdZnS , SnS_2) [8–10] photocatalysts have suitable band gaps (2.2–3.2 eV) and valence and conduction band levels to harvest the visible light region of the solar spectrum. In this way, they have the advantage of possessing greater efficiency of H_2 by splitting water as compared to metal oxides (TiO_2). Due to their low oxidation ability, sacrificial electron donors (SO_3^{2-}) as an oxidation reaction for photocatalytic H_2 production were used [6,7]. Amongst metal sulfides, SnS_2 has an optimum band gap value of 2.2 eV. Because of this, it has a high potential to have a high H_2 production efficiency [11–13]. On the other hand, the rapid recombination of charge carriers, which lowers photocatalytic efficiency, is observed. Due to the enhanced recombination, only 10% of the excitons proceed through a photo-reduction incident [13]. Due to these desirable features mentioned above, studies on SnS_2 water splitting have increased rapidly in recent years, attracting the attention of researchers (Fig. 1). The number of publications related to “ SnS_2 and water splitting” in the Scopus database since 2012 is given in Fig. 1, which demonstrates that there is still a long way to go in terms of splitting water using SnS_2 as a photocatalyst [13].

The literature commonly follows the hydrothermal method to produce SnS_2 in studies exploring its photocatalytic characteristics. Several studies have been conducted on this topic.

In the literature, there are a few studies examining the photocatalytic properties of SnS_2 synthesized by the thermal sulfuration method, a simple and affordable process.

Zhao et al. [14] synthesized 3D flower like SnS_2 nanoplates using a hydrothermal procedure, with the process taking a total of 37 h and beginning with $\text{SnCl}_4 \cdot 5\text{H}_2\text{O}$ as the starting material. They calculated the band gap value of SnS_2 as 2.28 eV. In order to investigate the photoelectrochemical behavior they used an aqueous solution containing Na_2SO_4 as a sacrificial agent under 500 W Xe lamp irradiation with a 420 nm cutoff filter. The photocurrent density of SnS_2 was measured as $1.5 \mu\text{A}/\text{cm}^2$.

Geng et al. [15] used a hydrothermal route starting from $\text{SnCl}_4 \cdot 5\text{H}_2\text{O}$, with the procedure requiring 17 h for synthesizing SnS_2 which exhibited regular hexagonal nanosheet structures. After UV–vis diffuse reflectance spectra measurements, the band gap value of pristine SnS_2 was calculated as 1.99 eV. In photoelectrochemical experiments carried out in solutions containing Na_2SO_4 , SnS_2 showed a $1.4 \mu\text{A}/\text{cm}^2$ current density under 300 W Xe lamp illumination with a 420 nm cut-off filter.

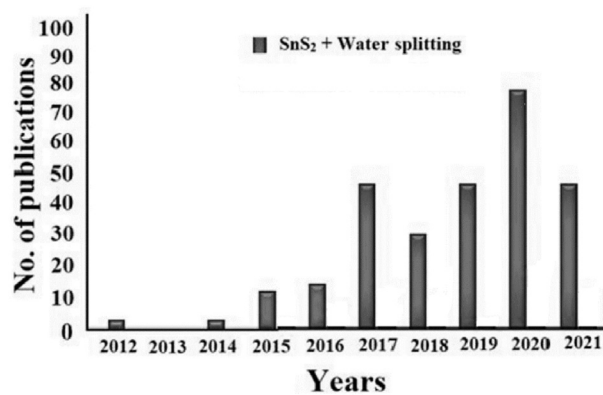


Fig. 1 – Number of publications found on Scopus using the keywords, “ SnS_2 + Water Splitting” [13].

Liu Y. et al. [16] synthesized hexagonal SnS_2 nanostructures using stannic chloride a thiourea as precursors in a hydrothermal method. They measured the indirect band gap of SnS_2 as 2.25 eV. In an aqueous solution containing 0.5 M Na_2SO_4 , the photocurrent response of SnS_2 photoelectrode was measured as $1.5 \mu\text{A}/\text{cm}^2$ with a 0.5 V bias vs. Ag/AgCl electrode under a 300 W Xe lamp irradiation with a 400 nm cutting of filter.

There were a few studies in the literature where sulfuration process was employed to produce SnS_2 photocatalysis.

In their study, Huang [17] and colleagues used SnS thin films as precursors. They sulfurized SnS thin films at 250°C for 2 h under a low vacuum with excess sulfur to produce hexagonal SnS_2 thin films. The obtained film's direct band gap value as 2.22 eV SnS_2 photoelectrodes showed $10\text{--}15 \mu\text{A}/\text{cm}^2$ photocurrent density under $100 \text{ mW}/\text{cm}^2$ irradiation in a 0.25 M H_2SO_4 solution at 0 V vs Ag/AgCl .

Liu et al. [18] synthesized pure SnS_2 nanosheets from Sn nanoparticles by the sulfuration method using elemental sulfur as a sulfur source in sealed tube glass that was placed in a tube furnace. They set the sulfuration temperature at 300°C and kept it there for 120 min. After that, they heat the obtained powder to 200°C for 120 min in an alumina crucible to remove excess sulfur. Synthesized powders show hexagonal crystal structures. They measured the band gap value of SnS_2 powders as 2.15 eV. For photoelectrochemical measurements, they used a 300 W Xe lamp with a 420 nm filter for illumination, and they prepared a 0.5 M Na_2SO_4 solution as an electrolyte. In photocurrent transient response measurements, they reported that SnS_2 sample show $1 \mu\text{A}/\text{cm}^2$ at a bias potential of 0.0 V vs. Ag/AgCl .

The study in this paper was aimed to fill this gap by examining the photocatalytic properties of SnS_2 synthesized from SnO_2 first time by a low-cost, one-step thermal sulfuration method. Also, it has been reported that in the author's previous work [8] photocatalysts synthesized by the thermal sulfuration technique displayed a distinct and exclusive hexagonal phase with high crystallinity, an absorption edge at the longest wavelength, and comparatively elevated photocatalytic activity in the absence of noble metal cocatalysts.

Within the scope of this study, it was aimed to synthesize SnS₂ photocatalyst to produce H₂ with high efficiency by splitting water via solar energy. The sulfurization parameters, such as exposure temperature and time, were optimized for obtaining the highest purity of the SnS₂ phase and eliminating SnO₂. The photoelectrochemical characterization techniques (chronoamperometry, linear-sweep voltammograms, Mott-Schottky plots, and open circuit potential under dark and illuminated conditions) were used to determine the PEC properties of SnS₂ photocatalysis.

2. Materials and methods

2.1. Synthesis of tin disulfide (SnS₂)

Tin disulfide (SnS₂) powders have been synthesized from tin oxide (SnO₂) nano powders (≤ 100 nm average particle size obtained from sigma Aldrich) by sulfurization using 99.9% pure sulfur powder in a Protherm hot-wall tube furnace at 400 and 500 °C to examine the effect of temperature on SnS₂ formation. Other phases (Sn₂S₃, SnS) are produced in sulfurization reactions conducted at 600 °C and above in addition to SnS₂ [20]. For these reasons, the temperature selected in the experiments did not exceed 500 °C. As indicated in Fig 2, 100 mg of SnO₂ powders were put in an alumina crucible and placed in the center of the heating zone, while the crucible containing elemental sulfur was placed outside of the heating zone at a temperature between 180 and 200 °C. The system was flashed with argon gas for 40 min before the furnace was heated. The furnace reached the desired temperature by heating at a rate of 10 °C/min and was kept constant at the desired temperature for 3-9-16-24 and 48 h under the flow of Ar gas at 400 °C and 500 °C. The rate of Ar gas flow was set to 0.15 L per hour. At the end of sulfurization, the furnace was switched off, and the powder was left to cool in the furnace to room temperature. Table 1 summarizes the processing parameters used for the sulfurization process.

2.2. Characterization of powders

X-ray diffraction measurement technique was used to identify the present phases and crystal structures of produced powder samples using a Bruker D2 Phaser. A Scan was performed between $10^\circ \leq 2\theta \leq 90^\circ$ using Cu-K α radiation of wavelength 1.5406Å. UV-vis spectrophotometry The PG

Table 1 – Process parameters for sulfurization process.

Temperature	500 °C	400 °C
Time	24–48 h	3-6-9-16-24 h
Atmosphere	Argon (0.15 lt/h)	
Sulfur Source	Elemental Sulfur	

Instruments T92+ test was performed to measure the band gap values of synthesized powders in the wavelength range of 300–900 nm. The surface morphology of the annealed thin films was examined using a Philips XL 30 SFEG SEM with an EDX attachment.

2.3. Photoelectrochemical measurements

The photoelectrochemical properties of SnS₂ were measured using a Biologic Potentiostat VMP-3 device and a three-electrode electrochemical cell. A platinum wire served as the counter electrode, and a standard calomel electrode was used as the reference electrode. The electrolyte used was an aqueous solution of 0.5 M Na₂SO₄. SnS₂ powders were coated onto FTO glass (1 cm × 1 cm) using the spin coating method to prepare the working electrode. 20 mg of SnS₂ powder was mixed with 2 ml of ethanol and stirred using an ultrasonic stirrer to form a suspension. The coated FTO glass was then heat treated at 100 °C for 1 h to volatilize the solvent and subsequently, annealed at 300 °C for 2 h to stabilize the sample. A solar simulator from ABET Technologies, equipped with a 150 W Xe lamp, was used for photoelectrochemical measurements (chronoamperometry, linear-sweep voltammograms, Mott-Schottky plots, and open circuit potential under dark and illuminated conditions) under 1 sun.

3. Results and discussion

3.1. XRD characterization of SnO₂ and SnS₂ powders

An XRD analysis was carried out after thermal sulfurization to confirm the success of the sulfurization process in the SnS₂ phase. The normalized XRD patterns of pure SnO₂ powders and SnS₂ powders synthesized at 400 °C for 3-9-16 and 24 h, respectively, were given in Fig. 3. The results showed that the success of the sulfurization of the SnO₂ powders increased with increasing sulfurization time. The XRD patterns of

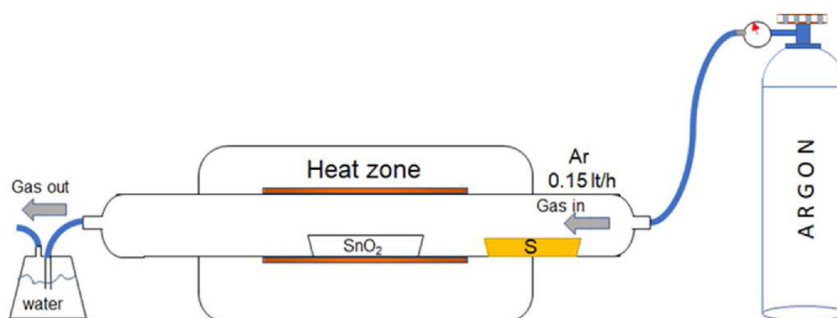


Fig. 2 – Schematic representation of a tube furnace for the thermal sulfurization of SnO₂ powders.

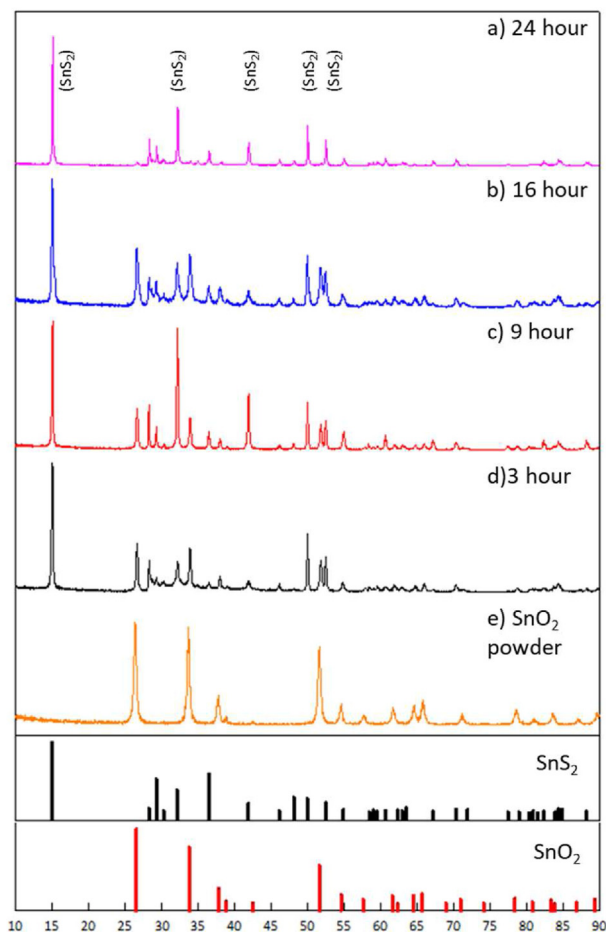


Fig. 3 – XRD patterns e) pure SnO_2 powders and after sulfuration at 400°C a)24 b)16 c)9 d)3 h.

samples obtained after sulfuration periods of 24 h revealed minor SnO_2 peaks compared to those of samples acquired after sulfuration times of 3-9-16 h at 400°C . The results indicated that sulfuration was completed with the appearance of major SnS_2 peaks in the XRD pattern in Fig. 3 (a) after sulfuration for 24 h at 400°C .

The XRD peaks obtained for the sulfurized samples at 500°C (Fig. 4). for 24 and 48 h gave almost identical diffraction peaks with the major SnS_2 peaks and minor SnO_2 peaks. The diffraction peaks of sulfurized powder at 400° for 24 h and 500°C for 48 h clearly proved the existence of a major SnS_2 phase having a hexagonal crystal structure with lattice parameters $a = 3,645$, $b = 3645$ and $c = 11,802 \text{ \AA}$ (PDF 01-089-2357). The major peaks of SnS_2 were detected at 15.13° , 32.13° , 41.87° , 50.05° and 52.5° . These peaks correspond to the (002), (102), (104), (110), and (112) planes of hexagonal structure, respectively.

An image of pristine SnO_2 and thermally sulfurized powder at 500°C for 24 h in an Ar atmosphere can be seen in Fig. 5. Due to the yellow color of SnS_2 , sulfuration of SnO_2 powders, white (Fig. 5a), to SnS_2 resulted in powders with yellow tones (Fig. 5b), as expected [19]. The success of sulfuration can be monitored by the change in powder colour. SnS_2 powders with

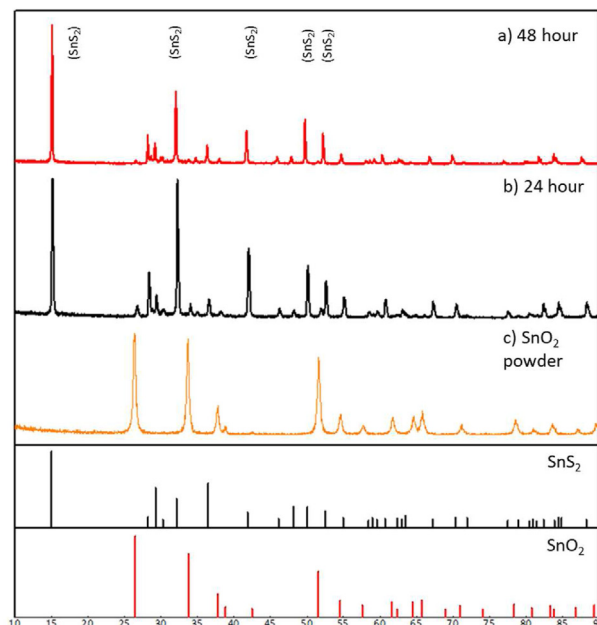


Fig. 4 – XRD patterns c) pure SnO_2 powder and SnO_2 powder safter sulfuration at 500°C a)24 b)48 h.

the major phases were successfully produced at 400°C for 24 h and 500°C for 24 and 48 h, respectively. The powders synthesized at 500°C for 24 h and 400°C for 24 h were further investigated by characterization methods (SEM and UV–Vis absorption spectroscopy).

3.2. Surface characterization of SnS_2 powders by SEM

The SEM surface morphology images of the pure SnO_2 powders before and after sulfuration at 400°C and 500°C for 24 h were displayed in Fig. 6. Pure SnO_2 (Fig. 6a) has nearly uniform spherical size of powders. In the SEM image of both SnS_2 (Fig. 6b-c) powders obtained by sulfurizing at different temperatures exhibited complete growth of hexagonally shaped flakes as identified by XRD patterns (Fig. 4). In Fig. 6(b and c) seen in the SEM images, the large surface area of hexagonally shaped flakes was believed to allow more efficient light absorption, resulting in increasing the efficiency of the photocatalytic reaction [20]. The grain size of the pure SnO_2 powder was below $<100 \text{ nm}$, as can be seen in the SEM images (Fig. 6a), whereas sulfurized powders had a larger grain size. Furthermore, the average size of SnS_2 particles obtained at a temperature of 500°C was $11 \mu\text{m}$, which was larger in comparison with the particle size obtained at 400°C which was $1 \mu\text{m}$. It was evident that as the sulfuration temperature increased, the particle size of SnS_2 powders increased.

To confirm the powder composition, SnS_2 synthesized at different temperatures was analyzed by energy dispersive X-ray (EDX) as shown in Table 2. According to an EDX analysis, before sulfuration, SnO_2 only contained tin and oxygen, and after sulfuration, the atomic ratio of Sn/S elements in SnS_2 powders synthesized at 400°C and 500°C , is 1:2.11 and 1:2.07, respectively, which was very close to the theoretical stoichiometry of SnS_2 . This result supported the XRD analysis and



Fig. 5 – Photograph SnO₂ powder a) Before sulfuration b) After sulfuration at 500 °C for 24 h.

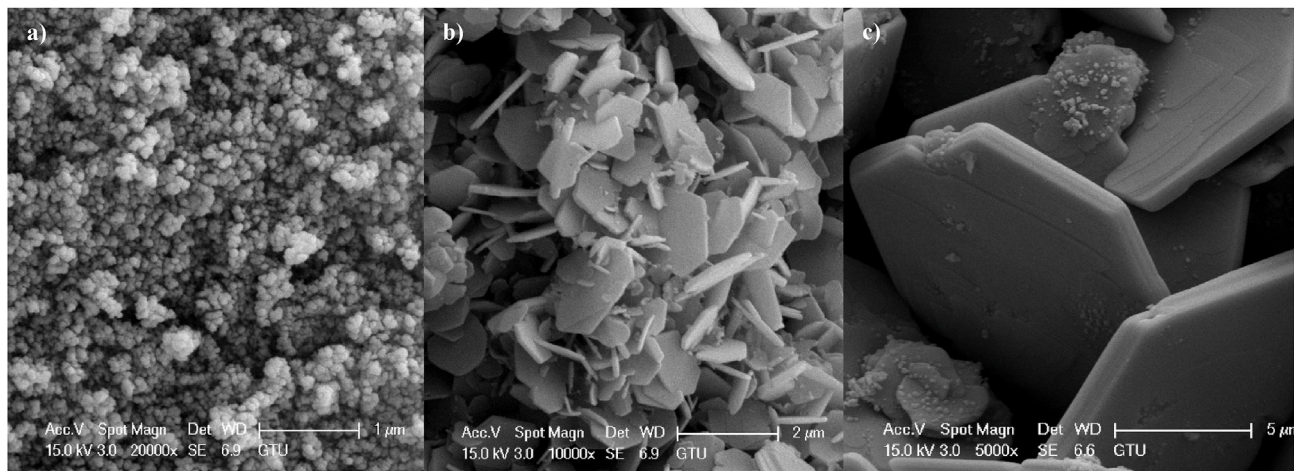


Fig. 6 – SEM Images of SnO₂ powders a) before and after sulfuration for 24 h b) at 400 °C and c) 500 °C.

the experimental findings by showing that the highly purified SnS₂ was effectively produced through thermal sulfuration.

3.3. Band gap measurement of SnS₂ photocatalyst

The band gap value (E_g) of the produced SnS₂ powder at 400 °C and 500 °C for 24 h was determined by measuring the powder spectrum absorption using UV–Vis absorption spectroscopy. In Fig. 7, the UV–Vis reflectance spectra and Tauc plot can be seen. The photoactivity of SnS₂ in the visible light region is indicated by the absorption edges observed at a wavelength of 550 nm, as depicted in Fig. 7a. The E_g value of SnS₂ powders was calculated by applying the Kubelka-Munz theory and drawing a Tauc plot using the data obtained from the UV–vis spectrometer measurement [21]. According to the Tauc plot, SnS₂ powder synthesized at 400 °C and 500 °C possessed an indirect band gap of around 2.26 eV and 2.24 eV respectively, which was within the expected range of earlier reported values in the literature [2.28 eV (14), 1.99 eV (15), 2.25 eV (16), 2.22 eV (17), 2.15 (18)]

Table 2 – EDX results after sulfuration at 400 °C and 500 °C for 24 h.

Samples	Elements	Atomic %
SnS ₂ – synthesized at 400 °C	Sn	32.09%
	S	67.91%
SnS ₂ – synthesized at 500 °C	Sn	32.51%
	S	67.29%

3.4. Photoelectrochemical characterization results

PEC results of SnS₂ photoelectrode produced from SnS₂ powders synthesized at 500 °C for 24 h were as follows. When the SnS₂ photoelectrode was illuminated in the neutral electrolyte, the measured open circuit potential (OCP) (Fig. 8a) shifted towards more cathodic potentials. The direction of the measured potential shift indicated that the SnS₂ photoelectrodes had n type semi conductivity, as indicated in the literature [22]. The OCP drop of the SnS₂ photoelectrode was observed as 120 mV in the electrolyte.

Mott-Schottky plot measurements were made to determine the carrier density and the flat band potential of the SnS₂ photoelectrode. The flat band potential of SnS₂ photoelectrodes was calculated by extending the linear portion of the Mott-Schottky plot (Fig. 8b) to the x-axis. The potential value of the flat band was determined to be -0.50 V. In addition, the slope of the Mott Schottky plot was positive, showing that the SnS₂ photoelectrodes had n-type conductivity, with electrons being the majority of carriers. Also, from the slope, charge carrier concentration was calculated according to Equation (1). [$\epsilon r_{(\text{SnS}_2)} = 17.7$] [17].

$$N_D = \frac{1.41 \times 10^{32} (\text{cm} \times F^{-2} \times V^{-1})}{\epsilon_r \times A^2 \text{cm}^4 \times (F^{-2} \times V^{-1})} \quad (1)$$

Then the charge carrier concentration of the SnS₂ photoelectrode was calculated as $1.49 \times 10^{20} \text{ cm}^{-3}$ which was higher than the other similar studies [$8.48 \times 10^{19} \text{ cm}^{-3}$ (14), $5.08 \times 10^{18} \text{ cm}^{-3}$ (16)].

The current-voltage response (linear sweep voltammetry) for the SnS₂ photoelectrodes under an applied voltage from

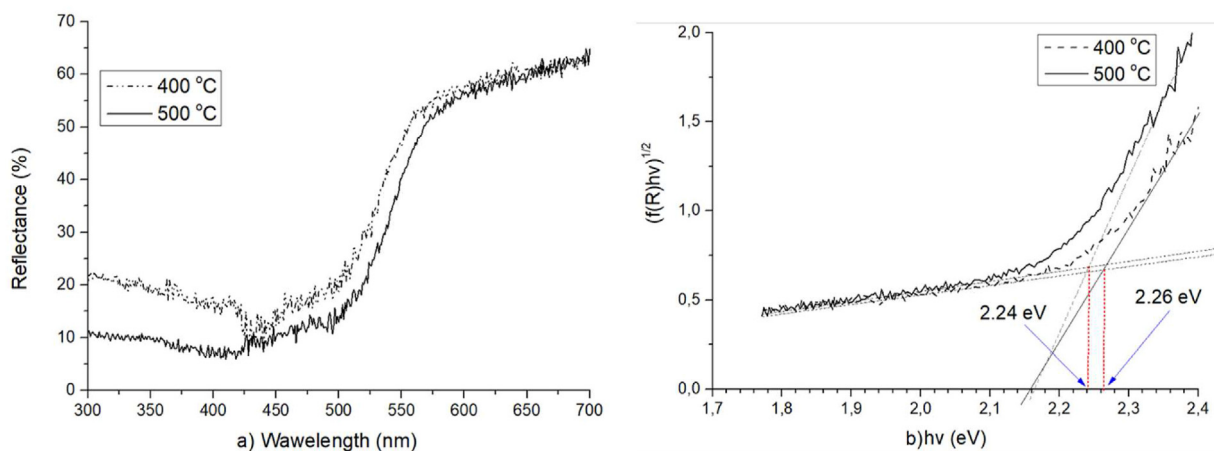


Fig. 7 – a) UV-Vis diffuse reflectance spectra of SnS₂ b) Tauc plot for determine the band gap of SnS₂.

–0.4 to 1.0 V during dark and illuminated conditions is given in Fig. 8c, demonstrating that a photocurrent was generated even without a bias potential (at OCP potential). This confirms that SnS₂ photoelectrodes are viable photocatalysts, as photoelectrochemical water splitting can occur without any external energy input.

The instantaneous photoresponse of the SnS₂ photoelectrode was investigated using chronoamperometry for both light on and off conditions during 250 s at 0 V vs SCE, (Fig. 8d). The photocurrent density value of the SnS₂ photoelectrode was measured to be 2.5 $\mu\text{A}/\text{cm}^2$. This value is higher than the other values that have been reported in the relevant literature

[1 $\mu\text{A}/\text{cm}^2$ (18), 1.5 $\mu\text{A}/\text{cm}^2$ (14), 1.4 $\mu\text{A}/\text{cm}^2$ (15)]. Furthermore, it is noteworthy that certain studies in the literature report higher photocurrents for SnS₂ photoelectrodes; however, it is important to acknowledge that these results were obtained under applied potential conditions. In a study conducted by Liu Y. et al. [16], a photocurrent density of 5 $\mu\text{A}/\text{cm}^2$ was measured for a SnS₂ photoelectrode at 0.5 V (Table 3). It is significant to mention that according to the linear sweep voltammograms (Fig. 8c), the measured current density value of around 20 $\mu\text{A}/\text{cm}^2$ which is four times higher than the value of the study conducted by Liu Y. et al. [16], was obtained in our investigation upon applying 0.5 V to the SnS₂ photoelectrode.

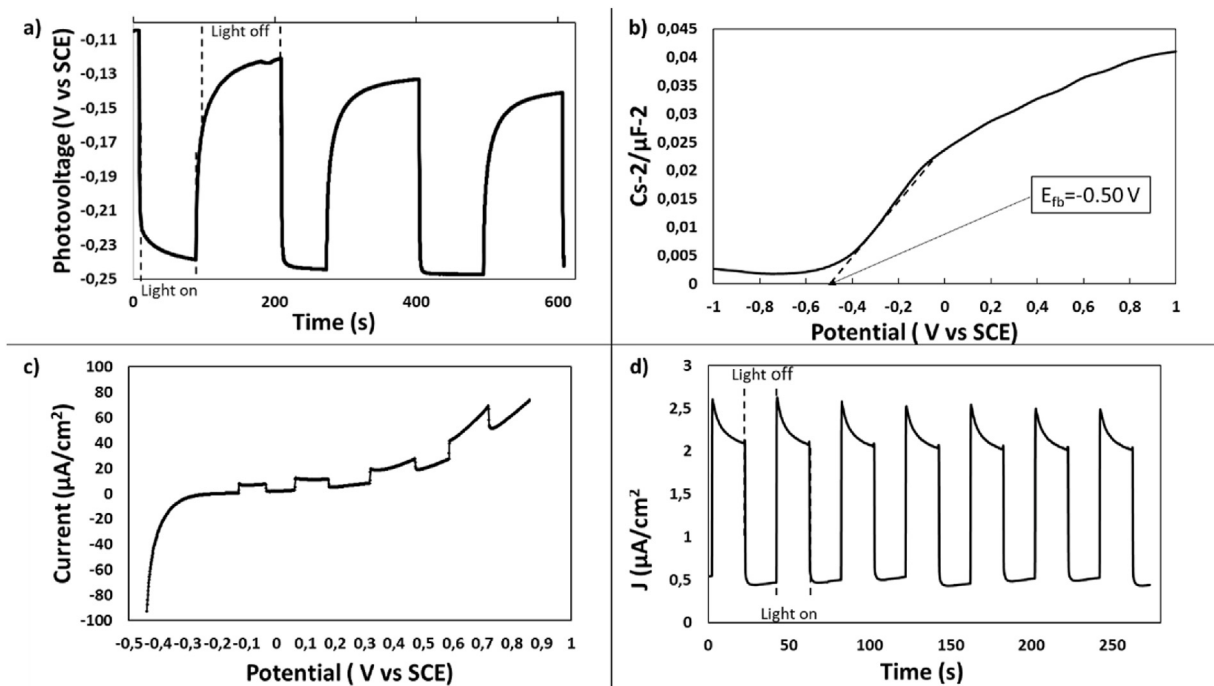


Fig. 8 – PEC Performance of SnS₂ powders after sulfurization at 500 °C for 24 h a) Open Circuit Potential under dark and illuminated conditions. b) Mott-Schottky plots c) Linear-sweep voltammograms from –0.4 V to 1 d) Chronoamperometry at 0 V vs SCE.

Table 3 – A representative summary of the performance of SnS₂ photoelectrodes stated in the literature.

Synthesizing Route	Band gap	Solution	Light	Photocurrent	Reference
Thermal Sulfurization	2.24 eV	Na ₂ SO ₄	1000 W/m ²	2.5 μA/cm ²	This work
Hydrothermal	2.28 eV	Na ₂ SO ₄	500 W Xe lamp	1.5 μA/cm ²	14
Hydrothermal	1.99 eV	Na ₂ SO ₄	300 W Xe lamp	1.4 μA/cm ²	15
Hydrothermal	2.25 eV	Na ₂ SO ₄	300 W Xe	5 μA/cm ^{2V} 0.5 V vs Ag/AgCl	16
Sulfurization from Sn nanoparticles	2.15 eV	Na ₂ SO ₄	300 W Xe	1 μA/cm ²	18

Table 3. represents the performances of some SnS₂ photoelectrodes stated in the literature. As shown in the table there are different SnS₂ synthesizing methods.

The band gap values of SnS₂, as reported in the studies mentioned earlier, exhibit minimal variation. The photocurrent density values are observed to be dependent on the experimental conditions. In comparison to similar studies reported in the literature (Table 3), the photocurrent value of SnS₂ (2.5 μA/cm²) in this particular study exhibits greater performance compared to its counterparts with and without an applied potential.

4. Conclusion

- 1 The present research examined the photocatalytic characteristics of SnS₂ powders that were produced through thermal sulfurization of SnO₂, indicating the first example of such a study in the literature.
- 2 SnS₂ powders were successfully synthesized from SnO₂ powders in a tube furnace at 400 °C for 24 h and 500 °C for 24 and 48 h under the Ar atmosphere, and fully sulfurized hexagonal SnS₂ phases were confirmed via XRD analysis.
- 3 An examination of the powders grain size using a SEM revealed that the powders produced at temperatures of 400 and 500 °C had average grain sizes of 1 μm and 11 μm, respectively.
- 4 The band gap value of the produced powders was determined as 2.24–2.26 eV as an indirect band gap. With a 2.24–2.26 eV band gap, SnS₂ was an ideal choice for photocatalytic water splitting amongst the metal sulfides.
- 5 As a result of the photoelectrochemical analysis of the SnS₂ (obtained at 500 °C) photoelectrode produced using SnS₂ powders, it was measured that it has a flat band potential of –0.50 V with a 1.49*10²⁰ cm⁻³ charge carrier density (N_d).
- 6 The photocurrent density value of the SnS₂ photoelectrode was measured to be 2.5 μA/cm², higher than the value reported in the literature. This result indicates that SnS₂ photocatalysis is promising photocatalysis as low cost and efficient hydrogen production technique.
- 7 The thermal sulfurization method was utilized to produce SnS₂ powder, which exhibited a band gap value range similar to that reported in the literature. Also, the PEC characterizations revealed a higher charge carrier density in the SnS₂, and the photoresponse measurements conducted at 0 V vs SCE demonstrated a higher current density comparing with the literature.
- 8 For a future work, the optimization of sulfurization temperature and time for obtaining the highest efficiency of photocurrent density and hydrogen production will be

concluded after PEC characterization of photoelectrodes prepared from SnS₂ powders.

Declaration of competing interest

The authors declare that they have no known competing financial interests or personal relationships that could have appeared to influence the work reported in this paper.

Acknowledgement

This study was supported by Marmara University through the unit of scientific research project (BAPKO) (Project No: FDK-2021-10160).

REFERENCES

- [1] Ismail AA, Bahnemann DW. Photochemical splitting of water for hydrogen production by photocatalysis: a review. *Sol Energy Mater Sol Cell* 2014;128:85–101. <https://doi.org/10.1016/j.solmat.2014.04.037>.
- [2] Van de Krol R, Grätzel M. *Photoelectrochemical hydrogen production*, vol. 90. New York: Springer; 2012.
- [3] Dincer I, Joshi A. *Solar based hydrogen production systems*. Oshawa: Springer; 2013.
- [4] Harsito C, Triyono T, Rovianteo E. Analysis of heat potential in solar panels for thermoelectric generators using ANSYS software. *Civil Eng J* 2022;8(7):1328–38. <https://doi.org/10.28991/CEJ-2022-08-07-02>.
- [5] Laabid A, Saad A, Mazouz M. Integration of renewable energies in mobile employment promotion units for rural populations. *Civil Eng J* 2022;8(7):1406–34. <https://doi.org/10.28991/CEJ-2022-08-07-07>.
- [6] Di T, Xu Q, Ho W, Tang H, Xiang Q, Yu J. Review on metal sulphide-based Z-scheme photocatalysts. *Chem Cat Chem* 2019;11(5):1394–411. <https://doi.org/10.1002/cctc.201802024>.
- [7] Zhang K, Guo L. Metal sulphide semiconductors for photocatalytic hydrogen production. *Catal Sci Technol* 2013;3(7):1672–90. <https://doi.org/10.1039/C3CY00018D>.
- [8] Ayaz RZ, Akyüz D, Uğuz Ö, Tanşık İ, Saroğlu C, Karaca F, et al. Photoelectrochemical performance of thermally sulfurized Cd_xZn_{1-x}S photoanode: enhancement with reduced graphene oxide support. *Renew Energy* 2020;162:182–95. <https://doi.org/10.1016/j.renene.2020.07.102>.
- [9] Agopcan B, Akyüz D, Karaca F, Saroğlu C, Koca A. A new sulfur source for the preparation of efficient Cd_(1-x)Zn_xS photocatalyst for hydrogen evolution reaction. *Int J Hydrogen Energy* 2018;43(17):8206–20. <https://doi.org/10.1016/j.ijhydene.2018.03.104>.

- [10] Akyuz D, Ayaz RMZ, Yılmaz S, Uğuz O, Sarıoğlu C, Karaca F, et al. Metal chalcogenide based photocatalysts decorated with heteroatom doped reduced graphene oxide for photocatalytic and photoelectrochemical hydrogen production. *Int J Hydrogen Energy* 2019;44(34):18836–47. <https://doi.org/10.1016/j.ijhydene.2019.04.049>.
- [11] Gedi S, Minnam RVR, Kotte TRR, Park C, Kim WK. Fundamental aspects and comprehensive review on physical properties of chemically grown tin-based binary sulfides. *Nanomaterials* 2021;11(8):1955. <https://doi.org/10.3390/nano11081955>.
- [12] Su R, Besenbacher F, Hutchings G. Alternative materials to TiO₂. In: Colmenares JC, Xu YJ, editors. *Heterogeneous photocatalysis*. Berlin: Springer; 2016. p. 109–49. <https://doi.org/10.1007/978-3-662-48719-8>.
- [13] Sharma K, Patial S, Singh P, Khan AAP, Saini V, Nadda AK, et al. Strategies and perspectives of tailored SnS₂ photocatalyst for solar driven energy applications. *Sol Energy* 2022;231:546–65. <https://doi.org/10.1016/j.solener.2021.11.041>.
- [14] Zhao W, Li Y, Zhao P, Zhang L, Dai B, Xu J, et al. Novel Z-scheme Ag-C₃N₄/SnS₂ plasmonic heterojunction photocatalyst for degradation of tetracycline and H₂ production. *Chem Eng J* 2021;405:126555. <https://doi.org/10.1016/j.cej.2020.126555>.
- [15] Geng Y, Zou X, Lu Y, Wang L. Fabrication of the SnS₂/ZnIn₂S₄ heterojunction for highly efficient visible light photocatalytic H₂ evolution. *Int J Hydrogen Energy* 2022;47(22):11520–7. <https://doi.org/10.1016/j.ijhydene.2022.01.176>.
- [16] Liu Y, Zhou Y, Zhou X, Jin X, Li B, Li J, et al. Cu doped SnS₂ nanostructure induced sulfur vacancy towards boosted photocatalytic hydrogen evolution. *Chem Eng J* 2021;407:127180.
- [17] Huang PC, Shen YM, Brahma S, Shaikh MO, Huang JL, Wang SC. SnS_x (x= 1, 2) nanocrystals as effective catalysts for photoelectrochemical water splitting. *Catalysts* 2017;7(9):252. <https://doi.org/10.3390/catal7090252>.
- [18] Liu Q, Liu S, Wu A, Huang H, Zhou L. SnS₂ and SnS/SnS₂ heterojunction nanosheets prepared by in-situ one-step sulfurization and visible light-assisted electrochemical water splitting properties. *J Alloys Compd* 2020;834:155174. <https://doi.org/10.1016/j.jallcom.2020.155174>.
- [19] Park JC, Lee KR, Heo H, Kwon SH, Kwon JD, Lee MJ, et al. Vapor transport synthesis of two-dimensional SnS₂ nanocrystals using a SnS₂ precursor obtained from the sulfurization of SnO₂. *Cryst Growth Des* 2016;16(7):3884–9. <https://doi.org/10.1021/acs.cgd.6b00447>.
- [20] Zvavamwe F. *Production of tin sulphide (SnS) for photovoltaic applications*. Turkey: Marmara University; 2019. Master Thesis.
- [21] Landi JS, Segundo IR, Freitas E, Vasilevskiy M, Carneiro J, Tavares CJ. Use and misuse of the Kubelka-Munk function to obtain the band gap energy from diffuse reflectance measurements. *Solid State Commun* 2022;341:114573. <https://doi.org/10.1016/j.ssc.2021.114573>.
- [22] Fang F, Li H, Yao H, Jiang K, Liu Z, Lin C, et al. Two-Dimensional hybrid composites of SnS₂ nanosheets array film with graphene for enhanced photoelectric performance. *Nanomaterials* 2019;9(8):1122. <https://doi.org/10.3390/nano9081122>.